Video Article

Automated Quantification of Hematopoietic Cell – Stromal Cell Interactions in Histological Images of Undecalcified Bone

Sandra Zehentmeier[1], Zoltan Cseresnyes[2,3], Juan Escribano Navarro[4], Raluca A. Niesner[2], Anja E. Hauser[1,5]

[1]Immunodynamics, German Rheumatism Research Center, a Leibniz Institute

[2]Biophysical Analytics, German Rheumatism Research Center, a Leibniz Institute

[3]Max-Delbrück Center for Molecular Medicine

[4]Wimasis GmbH

[5]Immunodynamics and Intravital Imaging, Charité - University of Medicine

Correspondence to: Anja E. Hauser at hauser@drfz.de

URL: https://www.jove.com/video/52544
DOI: doi:10.3791/52544

Keywords: Developmental Biology, Issue 98, Image analysis, neighborhood analysis, bone marrow, stromal cells, bone marrow niches, simulation, bone cryosectioning, bone histology

Date Published: 4/8/2015

Citation: Zehentmeier, S., Cseresnyes, Z., Escribano Navarro, J., Niesner, R.A., Hauser, A.E. Automated Quantification of Hematopoietic Cell – Stromal Cell Interactions in Histological Images of Undecalcified Bone. *J. Vis. Exp.* (98), e52544, doi:10.3791/52544 (2015).

Abstract

Confocal microscopy is the method of choice for the analysis of localization of multiple cell types within complex tissues such as the bone marrow. However, the analysis and quantification of cellular localization is difficult, as in many cases it relies on manual counting, thus bearing the risk of introducing a rater-dependent bias and reducing interrater reliability. Moreover, it is often difficult to judge whether the co-localization between two cells results from random positioning, especially when cell types differ strongly in the frequency of their occurrence. Here, a method for unbiased quantification of cellular co-localization in the bone marrow is introduced. The protocol describes the sample preparation used to obtain histological sections of whole murine long bones including the bone marrow, as well as the staining protocol and the acquisition of high-resolution images. An analysis workflow spanning from the recognition of hematopoietic and non-hematopoietic cell types in 2-dimensional (2D) bone marrow images to the quantification of the direct contacts between those cells is presented. This also includes a neighborhood analysis, to obtain information about the cellular microenvironment surrounding a certain cell type. In order to evaluate whether co-localization of two cell types is the mere result of random cell positioning or reflects preferential associations between the cells, a simulation tool which is suitable for testing this hypothesis in the case of hematopoietic as well as stromal cells, is used. This approach is not limited to the bone marrow, and can be extended to other tissues to permit reproducible, quantitative analysis of histological data.

Video Link

The video component of this article can be found at https://www.jove.com/video/52544/

Introduction

Due to recent rapid technological developments in microscopy, including optical imaging, the analysis of cells within the context of the whole tissue has become increasingly accessible for immunologists. The characterization of single cells in suspension represents a valuable and indispensable method to understand cellular and molecular function. However, the analysis of the cells within their (micro)-anatomical environment is essential for understanding the interactions between various cell types that collaborate in complex processes such as the development of immune responses.

While it is relatively easy for microscopists to obtain qualitative information from images, it remains a challenge to quantify these data, partly due to the fact that analysis methods in this field are lagging behind compared to what is possible in image acquisition. Many researchers still rely on time-consuming manual cell counting in their histology images, thus introducing a bias amongst different raters and hindering replication by other groups. Oftentimes, one representative image is chosen to underline a statement on cellular position or co-localization in a publication, making it hard for the reader to judge the statistical relevance of such an event.

Together with the fact that the full information content of image data is rarely exploited, this emphasizes the need for a more unbiased, faster and comprehensive approach to analyze histological images.

The bone marrow is a complex tissue, which takes on important vital functions as the organ of hematopoiesis in adult vertebrates. Besides being the birthplace for hematopoietic cells[1,2] and playing an important role in B lymphocyte development[3], it also acts as a site where immune reactions are initiated[4] and supports mature, recirculating B cells[5]. In addition, its role in maintaining immunological memory has become increasingly appreciated in the last decade, as several types of cells constituting immune memory have been found to reside there[6-9].

The relation between the complex tissue architecture of the bone marrow and its functions still remain elusive. Unlike secondary lymphoid organs, which are organized in macro-compartments such as T and B cell zones, the bone marrow lacks a clear macro-compartmentalization.

So far distinct compartments in bone marrow are defined by their proximity to the bone cortex or to vasculature. The importance of the various resident stromal cell populations in the bone marrow for a number of processes such as supporting stem cells, development of B cells or maintenance of immune memory cell populations (such as long-lived plasma cells (PCs), $CD4^+$ and $CD8^+$ memory T cells) clearly indicates that there is a certain degree of micro-compartmentalization in the bone marrow.

These observations have led to the concept of distinct microanatomical niches, which are specialized in certain functionalities (stem cell maintenance, B cell development at various stages, and maintenance of immunological memory) in the bone marrow. Although there seems to be a certain degree of heterogeneity among the niches that serve different functions, some of the factors produced by stromal cells, such as CXC-chemokine ligand 12 (CXCL12) or interleukin 7 (IL-7), are crucial components for several of these niches[10]. The visualization and characterization of stromal cells in the bone marrow is difficult due to their morphological features with long, thin dendritic extensions forming a network throughout the bone marrow, and the lack of appropriate markers to discriminate stromal subpopulations.

It is not yet clear as to what extent these niches share common features with respect to their cellular and molecular composition, and which elements render a certain niche unique. In addition to stromal cells, hematopoietic cell types have been shown to play a crucial role by providing certain signals at least for some of the niches. Clearly, the complexity of the niche composition requires their analysis *in situ*, and it has become increasingly important for immunologists and hematologists to zoom in on bone marrow microarchitecture, *e.g.,* by analyzing the spatial relationships between its cellular components.

Here, a strategy to quantify cellular co-localization and neighborhood relationships in the bone marrow in an automated and unbiased way is presented. A detailed workflow including the generation of chimeric mice, harboring fluorescent stromal cells and non-fluorescent hematopoietic cells, preparation of histological sections from undecalcified bones, acquisition of confocal images covering the whole bone, as well as the automated image analysis of cellular co-localization and its validation/discrimination from random positioning by a simulation tool is provided (**Figure 8**).

Protocol

The animal experiments were approved by the appropriate state committees for animal welfare (Landesamt für Gesundheit und Soziales, Berlin) and were performed in accordance with current guidelines and regulations (animal experiment license G0194/11).

1. Generation of Fluorescent Bone Marrow Chimeric Mice

NOTE: The generation of fluorescent bone marrow chimeric mice to visualize bone marrow stromal cells is performed as described before[9].

1. Start treating Del-Cre x ROSA-tdRFP mice (mice expressing tandem red fluorescent protein (tdRFP) ubiquitously[11-13]) to prepare them for irradiation. Alternatively, use any other strain with ubiquitous expression of fluorescent protein. Administer 1 mg/ml of Neomycin and 1 mg/ml of vitamins (A, D3, E, C) via the drinking water two days before irradiation.
2. Irradiate mice twice with 3.8 Gray with a Cesium-137 gamma-irradiator within an interval of 3 hr. For this, place mice in an irradiation pie cage suitable for the respective irradiator.
   NOTE: For irradiation of mice, our Institute does not require anesthesia. Follow local Institutional policies regarding anesthesia for irradiation. Treat animals with 5 mg/kg of carprofen subcutaneously (s.c.) per day after the irradiation if there are signs of pain.
3. The next day, reconstitute mice by an intravenous injection of 3×10^6 bone marrow cells prepared from long bones of C57BL/6 donor mice in transfer buffer[9]. Keep the mice on Neomycin and vitamins for up to 2 weeks and monitor their well-being and weight during this time. Wait at least 4 weeks to allow for reconstitution of the immune system before starting the specific experimental treatments (*e.g.*, immunization)[9].
4. Sacrifice mice and place them on a dissection board, sterilize the legs with 70% ethanol. Euthanize mice in accordance with local Institutional policies. Our Institute performs cervical dislocation.
5. Use forceps and scissors to remove the skin from the thighs. Remove muscle tissue to expose the femoral bone. Luxate the femoral bone from the hip and knee joint using forceps and scissors. Be careful not to break or cut the bone.
6. Carefully remove remaining large pieces of muscle tissue and cartilage from the bone using scissors. Remove remaining muscle tissue by rubbing the bone with laboratory tissue paper. Collect the cleaned bones in a petri dish with phosphate buffered saline (PBS).
7. Fix whole femoral bones in 4% paraformaldehyde (PFA, electron microscopy-grade) for 4 - 6 hr.
8. Discard PFA and incubate bones in 10% sucrose in PBS O/N. The next day, incubate the bones in 20% sucrose O/N. The day after, incubate the bones in 30% sucrose O/N.

2. Cryosectioning of Bones

NOTE: After 16 - 24 hr in 30% sucrose, freeze bones and cryosection them according to Kawamoto's tape method[14,15].

1. Prepare a large beaker (2,000 ml volume) with dry ice and acetone (approximately 2:1 volume ratio, *e.g.,* 400 ml of dry ice and 200 ml of acetone) under a fume hood. Place a small beaker (150 - 250 ml volume) with hexane inside (30 - 50 ml approximately). Wait for the mix to cool down (approximately 10 min, until frost appears on the outside of the large beaker).
2. Fill ¾ of the labeled cryomold with Super Cryoembedding Medium (SCEM); carefully place the bones inside until they are fully immersed, taking care that they do not touch the edges of the mold. With large forceps hold the cryomold into the beaker with the bottom of the mold just touching the surface of the hexane.
   1. Let the outer edges of the SCEM freeze (indicated by opacity, this takes approximately 15 sec). Then fully drop the mold into the hexane and let it freeze for 1 - 2 min. Take out the frozen sample and wrap in cellophane and then aluminum foil (to protect the sample from drying out and to avoid exposure to light). Store at -80 °C until cryosectioning.
3. For cryosectioning of femoral bones use a standard microtome and microtome blades for hard tissues.
4. Set the sample and blade temperature of the microtome to -24 °C. Let the sample sit inside the microtome for about 15 min before cutting.

1. Fix the sample block to the metal sample holder with SCEM or optimal cutting temperature (OCT) medium. Adjust the orientation of the block if necessary. Trim the sample until the bone is fully opened and the marrow is visible. Adjust the section thickness to 7 µm (discard the first section).
2. Fix a piece of Kawamoto tape with the sticky side on the top of the sample block using a deer leather-covered wooden spatula. Subsequently, cut the sample and turn the tape so that the section is positioned on the top side. Transfer the tape to a slide glass using forceps. Fix the tape to the slide glass with Scotch tape.

5. Let sections dry for at least 30 min and store them at -80 °C until usage. Store unstained and unmounted slides in plastic slide boxes with spacers between single slides in order to avoid that they stick together. Stained and mounted slides can be stored for up to a week in cardboard slide folders at 4 °C.

3. Image Collection

1. Thaw and stain cryosections according to common immunofluorescence protocols[9]. Include a nuclear stain, *e.g.,* 4',6-diamidino-2-phenylindole dihydrochloride (DAPI) to visualize tissue integrity.
   NOTE: Stain, for example, for RFP to visualize stromal cells (anti-RFP-biotin antibody and streptavidin-Alexa Fluor 555), stain eosinophils with rat anti-major basic protein (MBP) antibody and anti-rat-Alexa Fluor 647 antibody, B cells with rat anti-B220-Alexa Fluor 594 antibody and PCs with anti-κ light chain-fluorescein-iso-thiocyanate (FITC) and anti-λ1 light chain-FITC antibodies (details of the staining procedure are described in[9]).
2. Mount stained sections: put one drop of fluoromount on the section and then cover with a #1 glass cover slip, whilst carefully avoiding the formation of air bubbles. Subsequently, perform laser scanning confocal microscopy with an instrument equipped with laser lines suitable for the staining.
3. In order to record images for automated co-localization analysis of bone marrow hematopoietic cells with stromal cells using the Wimasis tool, apply the following settings:
   1. Use a 20X objective lens and a field of view of 708.15 x 708.15 µm. For automated analysis, keep the size of all images consistent at 2,048 x 2,048 pixel (px) in order to keep the results comparable.
   2. Record one channel for stromal structures (*e.g.,* 561 nm laser line), one channel for nuclei (*e.g.,* DAPI, 405 nm) and additional channels for the hematopoietic cells of interest (*e.g.,* 3 channels, 488/594/633 nm for eosinophils, B cells and PCs).
   3. Record images using line averaging 4 [16]. Ideally, cover the whole femoral section by taking single adjacent images. Alternatively, take non-adjacent pictures from various regions of the bone marrow (diaphyseal as well as epiphyseal).
      NOTE: Be careful not to produce overlaps between adjacent images (to avoid repeated analysis of cells in the overlapping areas).

4. Save the images in a microscopy image file format. Check and, if necessary, adjust contrast for all channels in the image viewer/analysis software.
5. Export 3 .jpg files per image file: one .jpg file for the DAPI channel (red/green/blue (RGB) format, false color coded in yellow), one .jpg file for the stroma channel (greyscale) and one .jpg file containing the channels for hematopoietic cells (3 channels maximum, RGB format, *e.g.,* FITC (PCs, false color: green)/ Alexa Fluor 594 (B cells, false color: blue) / Alexa Fluor 647 (eosinophils, false color: red)).

4. Automated Image Analysis

1. Use an image analysis tool to perform image segmentation, quantification of co-localization and neighborhood analysis (see **Discussion**).
2. If using the Wimasis tools, proceed as follows:
   1. Upload the sets of 3 .jpg files per image with the same file name followed by an underline and a number indicating the type of the image.
   2. Use _1 for the .jpg file with hematopoietic cells, _2 for the .jpg file for the DAPI channel, _3 for the .jpg file for the stroma channel. For example: Image1_1.jpg (hematopoietic cells), Image1_2.jpg (DAPI channel), and Image1_3.jpg (stroma channel). Upload the images via the customer account.
   3. For cell contact quantification choose the cell contact tool by clicking on the respective field. For cell vicinity quantification, choose the cell vicinity tool and enter the preferred vicinity radius in µm (which is measured from the cells' edges).
   4. Download the results.
      NOTE: The results are provided as .jpg files showing the hematopoietic cells and the stroma channel with the boundaries of the detected objects highlighted, as well as single .csv files containing the measurements for every image, in addition to a summary .csv file that contains the data for all uploaded images.

3. From the contact measurements determine the frequency of hematopoietic cells (red, green, or blue cells) in contact with stromal cells, or the frequencies of red, green, or blue cells contacting the other hematopoietic cell types (an example is shown in Representative Results, **Figure 4**). In order to determine the frequencies, divide the given contact counts per image by the total cell counts per image.
   1. For experiments with individual mice, sum up the total contact counts of all images for the single mice and divide them by the sum of total cell counts of all images.

4. From the vicinity measurements, determine the frequency of red, green or blue cells within the selected distance from stromal cells and/or the frequencies of red, green or blue cells in the preferred proximity to the other hematopoietic cell types as described in step 4.3 (see also Representative Results, **Figure 4**).

5. Simulation of Random Bone Marrow Positioning

1. Before executing the simulations of random cell positioning on the analyzed bone marrow histological images, prepare the following files in advance: the single .csv files provided by the cell contact tool, the original .jpg files for the DAPI channel and the original .jpg files for the stromal channel.
2. In order to perform batch simulations on a series of images (*e.g.,* all images from one femoral section), collect all original .jpg files (_1, _2 and _3) and the corresponding single .csv files in one folder.
   NOTE: The simulation tool for random bone marrow cell positioning is available upon request.
3. Start the simulation tool, check the box “Auto-load image data”.
   NOTE: The program will read the cell counts and average cell size from the .csv file automatically. These values are displayed in the boxes for “Cell number” and “Cell size AVG” (**Figure 5A**).
4. Enter the common tag for the .csv files, *i.e.,* the common factor in their names. Enter the number of image sets that should be used for batch-mode simulation.
5. Load the .jpg file generated from the stroma channel (with filename ending _3).
6. Enter the settings for generating the mask from the DAPI channel:
   1. Check the box “Apply mask?” Set the threshold for converting the DAPI image into a binary mask to 10 (range 0 - 255).
   2. Check the box “8-bit?” Check the box “Dilate?” and set the grade of dilation to 5 px. Check the box “w/ erosion?”.
   3. Enter the desired value for the vicinity radius (neighborhood radius) used for the analysis of the simulated images. For an image of 708.15 x 708.15 µm with a size of 2,048 x 2,048 px (pixel scaling xy: 0.346 µm), 29 px correspond to 10 µm.
7. Check box “Use Otsu?” to use Otsu’s algorithm[17] for automatic detection of stromal structures.
   NOTE: This is the same algorithm that is used by the contact and vicinity tool. Using the same image segmentation algorithm in the automated analysis of the recorded image and the simulated image is crucial in order to keep the data comparable.
8. Enter the settings for hematopoietic cells, which are simulated as circular shapes.
   NOTE: The cell numbers for red, green, and blue cells are directly loaded from the .csv file (see also step 5.6).
   1. Use the simulation tool to calculate the average diameter in px of red, green and blue cells. Determine the average area of a single cell as the total area of each cell type in the image in px divided by the total cell count per image. Use the average area to calculate the radius of a disc using the formula. Double the radius to determine the average diameter.
9. Measure the cell size distribution of the analyzed cell types with any image analysis software that includes object segmentation functions. Determine σ for all hematopoietic cell types ([18] and **Figure 5B**).
   NOTE: Since the cell size distributions of the recorded cells are not determined by the automated image analysis, use a Gaussian distribution as an approximation of the real distributions. The width of the distribution curve is described by σ and can be quite different for various cell types. (For details, see **Figure 5B**).
   1. From these measurements, determine the “cell size cutoff”: the diameter in px that describes the smallest object still recognized as a complete cell by the image analysis tool.
10. Enter parameters in the respective boxes on the graphical user interface (**Figure 5A**).
    1. Enter the cell size cut off, *i.e.,* the minimum cell size allowed in the simulation, as a diameter in px.
    2. Enter σ in px for the simulation of the cell size distribution for red, green, and blue cells (from step 5.9).
    3. Check the “Delete” box in the subsection “Cells in Mask”. With this setting, the program will chose a new position for a cell if it overlaps with at least one pixel with a no-go area of the mask. Check the box “Avoid cell overlap?” in the subsection “Cell exclusion”.
    4. Enter the allowed minimum distance between the centers of two cells in px.
       NOTE: The minimum distance needs to be determined from the recorded images. Wrongly measured minimum distances will lead to biased/artificial results for the comparison of recorded and simulated images.
    5. Set the maximum area of overlap to 100% if the overlap is defined by the minimum distance from center to center.
    6. Set the simulation tool to 1,000 repetitions.
    7. Check the box “Autosave cells?” to save the coordinates of the simulated objects for all repetitions of each image of the batch as .rect files (text format). Check the box “Autosave images?” to save a .tiff file for each simulated image. Enter a common tag for the saved files.
       NOTE: The “Autosave cells?” option reduces simulation running time and overall data size, compared to when saving the actual simulated images. The .rect files save the coordinates of the simulated cells as rectangles and can thus be converted into simulated images if needed.
11. Start the simulation by clicking on “Run simulation”.
    NOTE: The simulation tool automatically generates a .csv file for the 1,000 simulations of every image, including the average contact counts and vicinity counts for red, green and blue cells with red, green, blue, and stromal cells for every set of repeated simulations. Additionally, for all these values, averages of the 1,000 simulations with standard deviation (STD) and standard error of mean (SEM) are provided.
12. Determine the average contact frequencies and vicinity frequencies of one set of 1,000 simulated images. For this, divide the average contact and vicinity counts by the recorded cell count per image. Compare the frequencies to the results of the automated co-localization analysis of the recorded image.
13. Apply appropriate statistical methods depending on the analysis[19] (for **Figure 7**, we used a two-tailed Wilcoxon signed rank test).

Representative Results

Cutting cryosections of undecalcified bone with the Kawamoto tape method allows the whole bone to be cut as an intact section, with the bone marrow of the endosteal region still attached to the mineralized bone, both in the diaphysis as well as in the epiphyseal areas with their high

density of trabecular bone (**Figure 1**). Nuclear staining of the sections reveals that although small cracks in the preparation cannot be fully avoided, the structure of the sinusoids and arteries as well as the reticular network of the parenchyma stays intact.

As an example of an immunofluorescence staining of red fluorescent chimeric bone marrow and its subsequent analysis, a staining for eosinophils (major basic protein, MBP), PCs (κ and λ light chain) and B cells (B220) is shown. Mice were immunized with 100 µg of 4-hydroxy-3-nitrophenylacetyl hapten coupled to chicken γ globulin (NP-CGG) in alum i.p., 4 weeks after reconstitution, boosted with 50 µg of NP-CGG in PBS i.v. 21 days later and analyzed on day 30 after the boost. The automated image analysis resulted in a very precise recognition of the stromal structures, including also very small fragments of reticular processes. Since the cell number of stromal cells cannot be determined with the system presented here (see also Discussion), no size threshold was introduced for the stromal channel, in order to detect all fragments in the images (**Figure 2**). PCs and eosinophils are larger than B cells and also show a more heterogeneous shape. All three cell types have been well recognized at first glance. Cellular clusters, especially of B cells, were well separated. The analysis tool is optimized for the above-mentioned cell types (eosinophils, PCs, B cells). For other cell types, adjustments might be necessary. The .csv files generated by the cell contact tool contain the following relevant measurements for hematopoietic cells: cell count for each cell population; total area for each cell population in px; contact count of red cells (in this case eosinophils), green cells (here PCs) or blue cells (here B cells) with red, green, blue or grey cells (stromal cells). The .csv files generated by the cell vicinity tool contain the following measurements for hematopoietic cells: cell count for each cell population; total area for each cell population in px; vicinity count of red, green, and blue cells with red, green, blue, and grey cells (stromal cells).

In order to validate the quality of the image analysis tools, the results of the automated analysis were compared to that of a manual counting by 6 trained raters (**Figure 3**). All raters received identical images for analysis. Stromal structures and hematopoietic cells were carefully outlined with an image analysis tool and these regions of interest were saved and analyzed. For stromal structures, the total area per image was compared between automated and manual analysis. Stromal structures seemed to be difficult for the trained raters to recognize precisely, as reflected by the large variance observed for the size of the total area of stroma counted manually (**Figure 3A**). Here, the automated analysis determined a value close to the average area detected by trained raters. For all cells, the automated analysis tool determined a slightly lower amount of cells than counted manually. However, for PCs and eosinophils, the number was still in the range of interrater variance observed for the manual counts. The number of B cells detected by automated analysis, however, was slightly below this range (**Figure 3A**). The average cell size (area in px) as determined by the automated analysis was 512 px for PCs, 436 px for eosinophils, and 317 px for B cells, while trained raters determined a size of 515 px for PCs, 464 px for eosinophils, and 291 px for B cells. Thus, the average cell size for B cells, PCs, and eosinophils determined by the automated analysis was comparable to the average cell sizes determined by manual raters (**Figure 3B**). This automated image analysis tool can now be used to quantify direct contacts of candidate bone marrow niche cell types. Moreover, the frequency of cells of a certain cell type neighboring stromal cells or other hematopoietic cells types can be determined. An analysis of bone marrow PCs and their contacts to stromal cells, eosinophils, B cells, and other PCs is shown, as well as the frequency of PCs neighboring these cell types within 10 and 20 µm (**Figure 4A**). Additionally, the contact frequencies of various hematopoietic cell types with stroma can be quantified (**Figure 4B**).

Before performing a simulation of random bone marrow positioning of these cells with the simulation tool, the parameters that describe the cell size distribution as a Gaussian distribution have to be determined. For a Gaussian distribution, which can be visualized as a symmetrical and "bell-shaped" curve, only two parameters need to be determined: the location of the center of the curve (the mode, *i.e.,* where the peak of the curve is located) and the width of the symmetrical curve (this is described by the above-mentioned σ parameter). This procedure is shown here for PCs, eosinophils, and B cells (**Figure 5B**). Measured cell size distributions show that, for B cells, the width of the distribution curve described by σ is smaller than for PCs and eosinophils. For the simulation, the relative values of σ measured for the three cell populations were maintained (*i.e.,* B cells were always simulated by a twice as narrow size distribution than that of PCs' and eosinophils'), while the σ values defined in px were set to match the visual appearance of the recorded cells (**Figure 6B**). This led us to apply an σ of 2 px for B cells and a σ of 4 px for both PCs and eosinophils. The cell size cutoff was determined from the measured cell size distributions. For PCs and eosinophils, a cutoff at 300 px object size, resulting in 20 px diameter for a circular object (about 7 µm) and for B cells a cutoff at 220 px, leading to a 17 px diameter (about 6 µm) was used for the simulation.

In order to define areas in the simulated random image where cells are allowed to be placed by the simulation tool, a mask was generated from nuclear signals in the DAPI channel of a bone marrow histological image (**Figure 6A**). A value of 10 was determined to be the optimal intensity threshold for generating the binary images (upper panel, right image). The threshold determined by Otsu's algorithm does not lead to full recognition of all nuclei in the image (upper panel, center image), similarly to fixed intensity thresholds of 50 or 150 (lower panel, left and center image).The relevance of contacts of PCs, eosinophils, or B cells with stromal cells (**Figure 4B**) was tested using the simulation tool (**Figure 7**). This analysis revealed significantly higher contact rates in the recorded images compared to the simulation for PCs and B cells (**Figure 7A**), in line with the concept of stromal niches supporting these populations. This was confirmed in 5 individual fluorescent chimeric mice (**Figure 7B,D**). In contrast, no clear difference was determined in the case of eosinophils (**Figure 7A,C**).

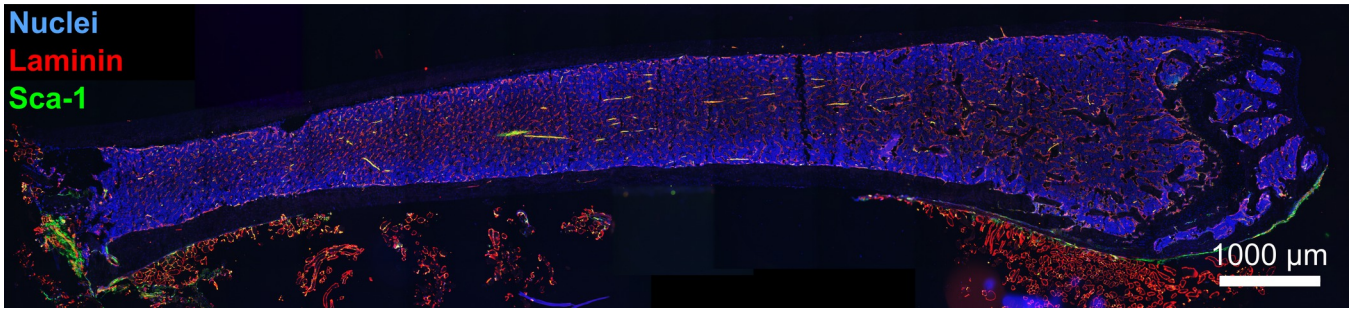

Figure 1. Overview fluorescence image of a longitudinal section of a murine femur cryosectioned with Kawamoto's tape method. The tape method allows cutting sections with an intact endosteal region, both in the diaphyseal as well as in the epiphyseal areas, from undecalcified bone. A 7 µm thick bone section of a naïve C57BL/6 mouse was stained for the extracellular matrix protein Laminin (red), for Sca-1 to visualize arterioles (green) and for nuclei (blue, DAPI). 47 tiles of 1,446 x 1,088 µm, resolution 1,360 x 1,024 px were recorded and stitched to create the overview image. This image was acquired on a wide-field fluorescence microscope, with a 10X objective lens (0.45 NA). Please click here to view a larger version of this figure.

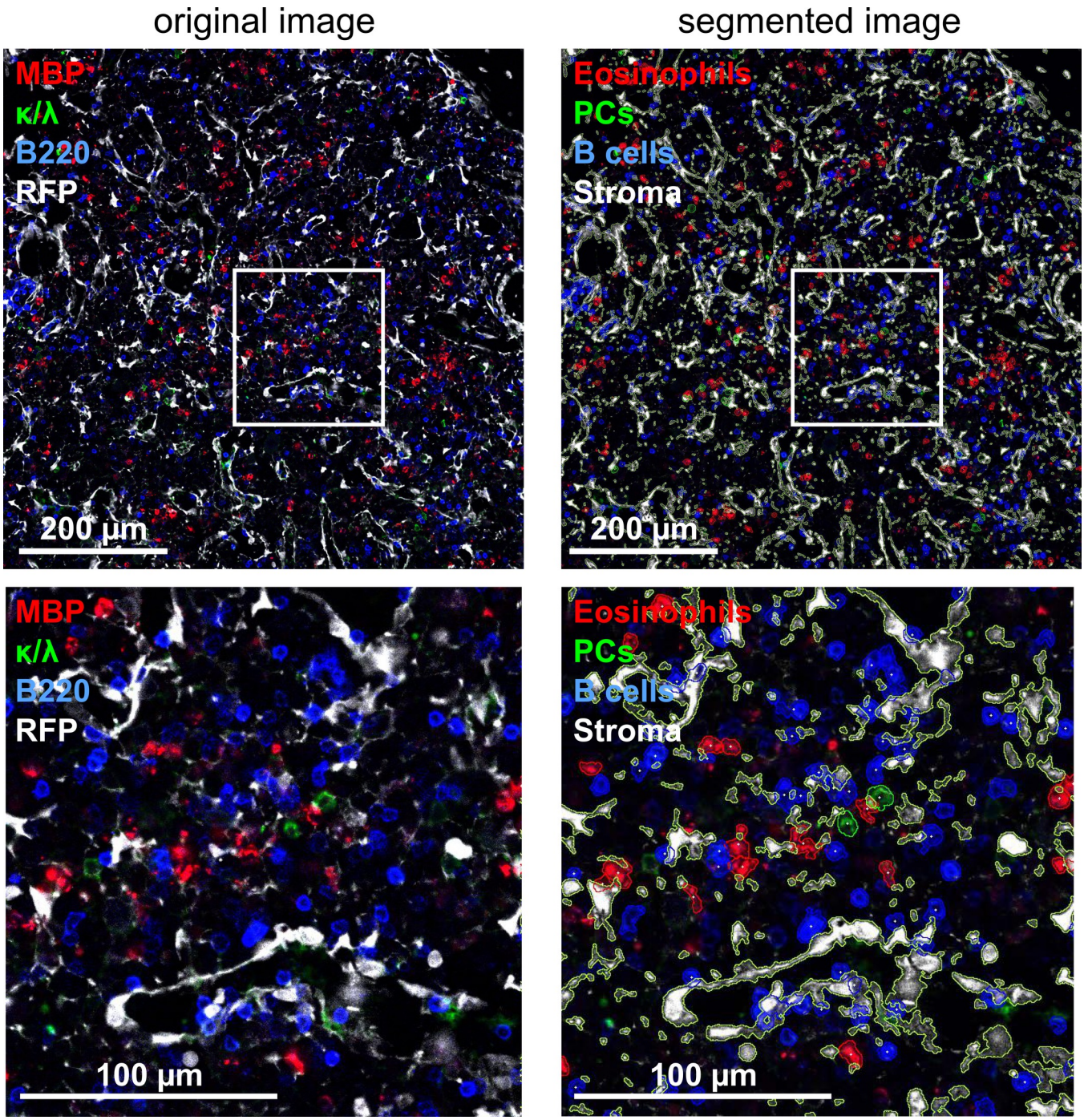

Figure 2. Automated detection of stromal and hematopoietic bone marrow cells. A femoral bone section of a red fluorescent chimeric mouse on day 30 after boost was stained for RFP (grey) to visualize stroma, MBP (red, eosinophils), κ and λ light chain (green, PCs) and B220 (blue, B cells). Left: Original image acquired on a confocal microscope, using a 20X objective lens (0.8 NA) and a field of view of 708.15 x 708.15 µm. Right: Segmented image. The outlines of the recognized objects are highlighted. The white rectangles mark the area shown in the bottom images. Please click here to view a larger version of this figure.

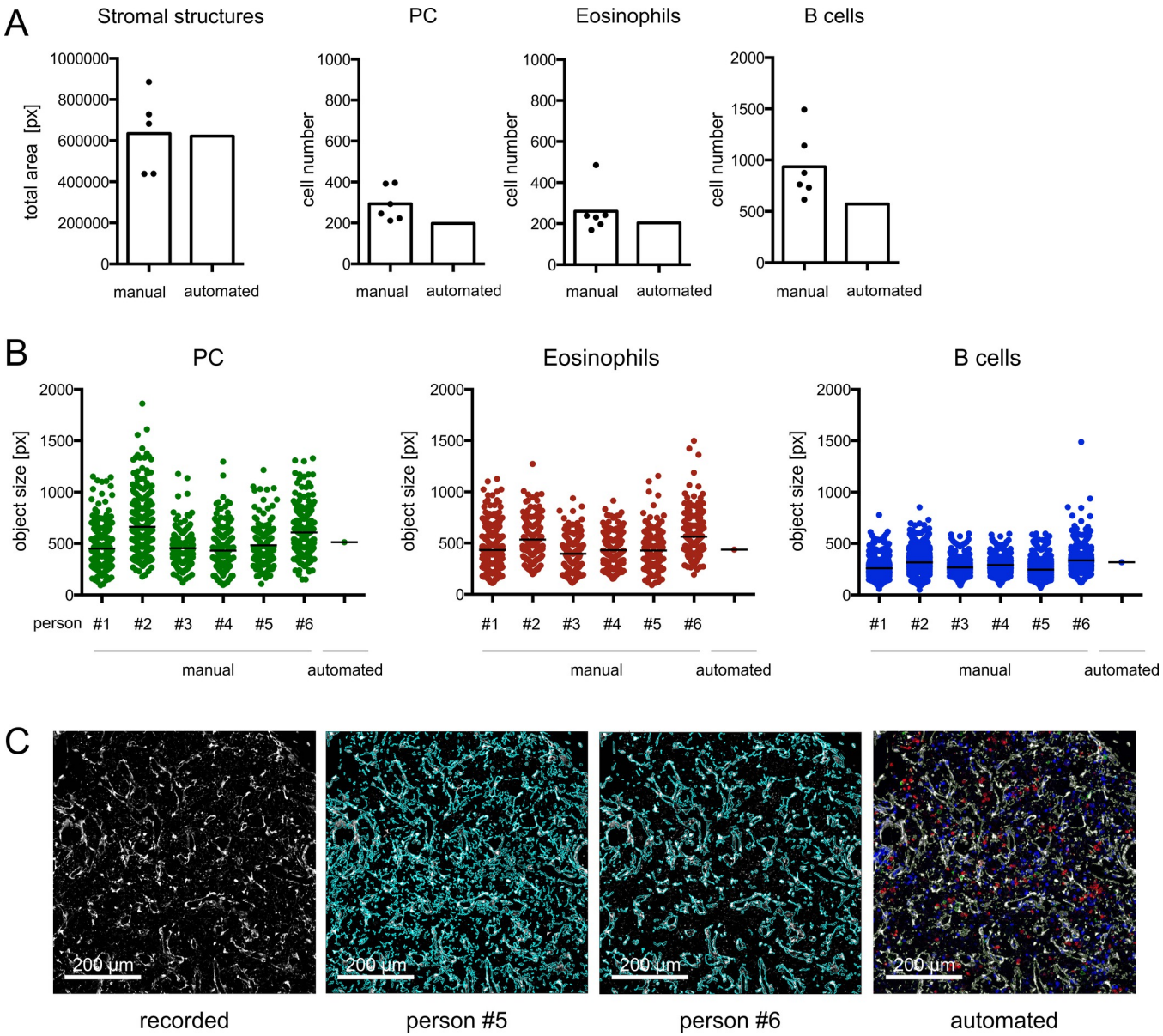

Figure 3. Validation of the automated image analysis by trained raters. (A) Total area of stromal structures and total cell numbers of hematopoietic cells counted by trained raters in one (stromal structures), 10 (PCs), two (eosinophils) and one image (B cells) compared to cell numbers obtained by automated image analysis. Dots represent individual raters (n = 5 - 6). Bars indicate mean values or automatically determined values. **(B)** Object size distribution of manually counted objects compared to the average object size determined by automated analysis. In order to account for the different frequencies of the various cell types, PCs were counted in 10, eosinophils in two and B cells in one image. Dots represent individual objects. Lines indicate mean. **(C)** Manual outlining of stromal structures by trained raters. Left: original image. Middle: examples of manually analyzed images. Right: stromal structures detected by automated analysis. Please click here to view a larger version of this figure.

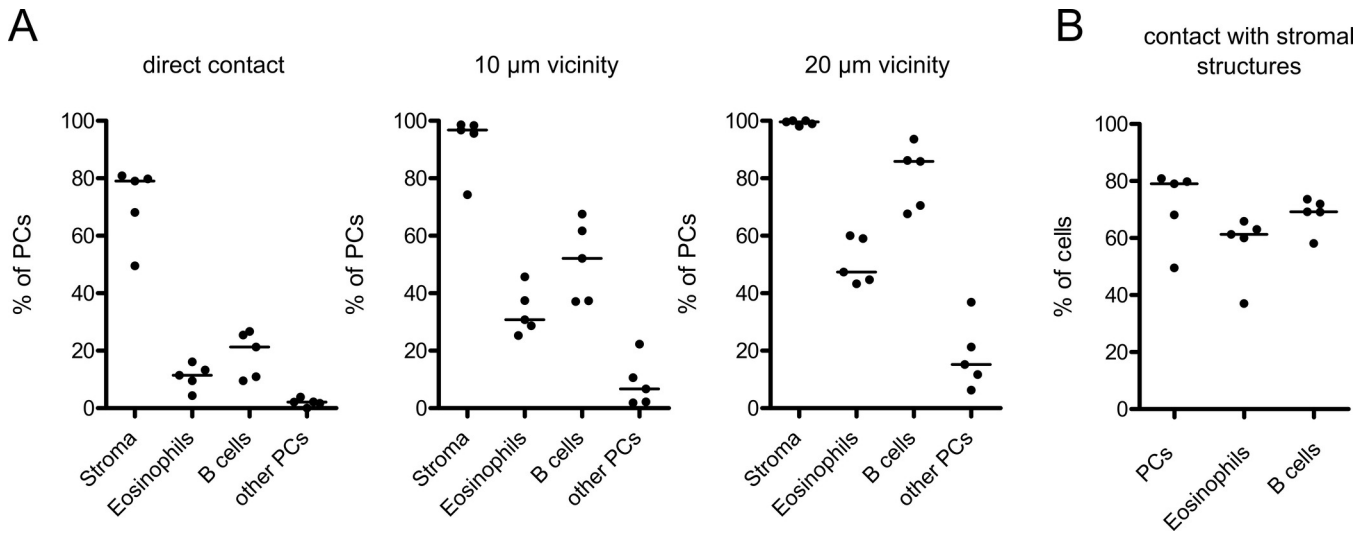

Figure 4. Automated co-localization analysis of PCs, eosinophils, B cells and stromal cells in the femoral bone marrow. (A) Left: Frequency of PCs in direct contact with stromal structures, eosinophils, B cells or other PCs in fluorescent chimeric mice on day 30 after the boost. Middle and right: Frequency of PCs in 10 µm vicinity or 20 µm vicinity of stromal structures, eosinophils, B cells or other PCs. Parts of this figure (direct contact, 10 µm vicinity) are modified from Zehentmeier *et al.*[9] **(B)** Frequency of PCs, eosinophils and B cells in direct contact with stromal structures. 52–515 PCs, 918-3179 eosinophils, 4146-13063 B cells in 10-21 images were counted from 5 fluorescent chimeric mice on day 30 after the boost, pooled from two independent experiments. Dots represent individual mice. Lines indicate median. Please click here to view a larger version of this figure.

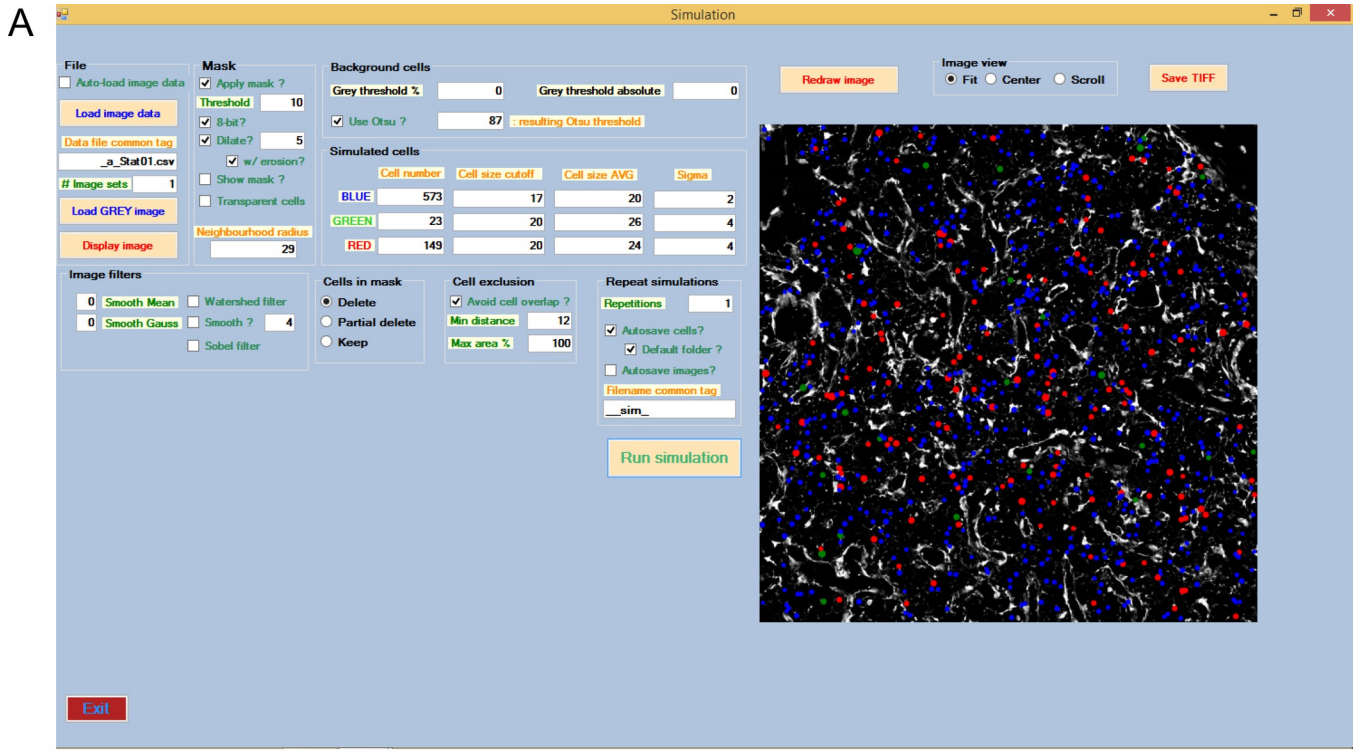

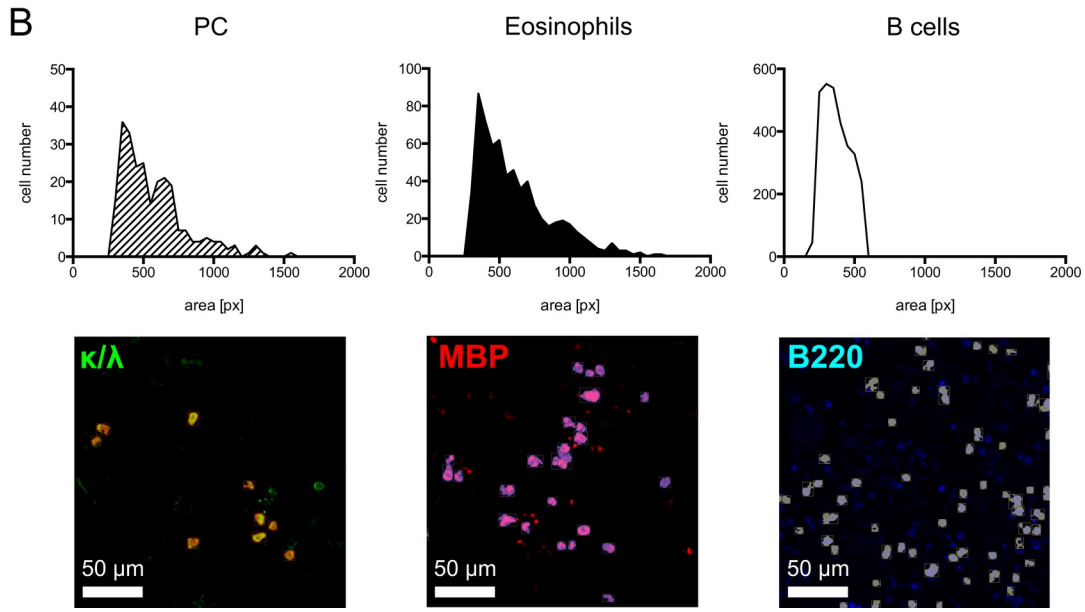

Figure 5. Determination of the cell size distribution of bone marrow PCs, eosinophils and B cells. (A) Screenshot of the graphical user interface (GUI) of the simulation tool. **(B)** The cell size distribution (area in px) of PCs (κ and λ light chain, green), eosinophils (MBP, red) and B cells (B220, blue) is shown in histograms as measured after object recognition by Volocity software (upper panel). In femoral bone marrow images (lower panel), detected PCs are marked in red (overlay yellow), eosinophils in blue (overlay violet) and B cells in yellow (overlay grey). Image segmentation was performed by setting a minimum size threshold of 180 px for PCs, 300 px for eosinophils and 220 px for B cells. 250 objects were measured for PC, 650 objects for eosinophils and 3,000 objects for B cells. Please click here to view a larger version of this figure.

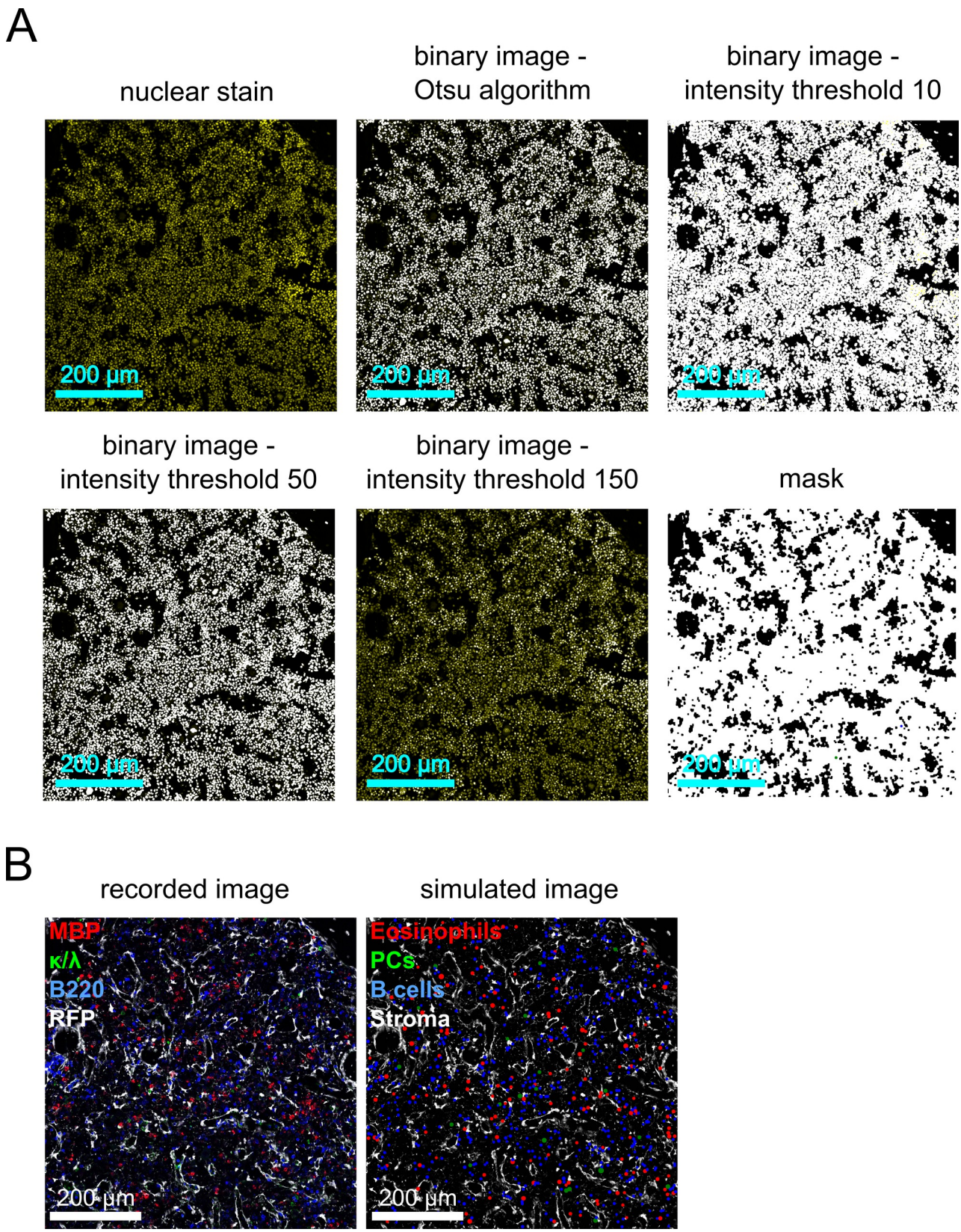

Figure 6. Generation of the mask for simulated random cell positioning. (A) The original DAPI channel (yellow) as well as overlays of DAPI with binary images generated by applying various thresholds are shown. The mask generated from the binary image (threshold set to 10) is displayed below (lower panel, right image). Black areas represent no-go areas, white areas represent areas where cells are allowed to be placed. **(B)** The recorded image (left) and the corresponding simulated image (right) show high visual similarity. Eosinophils (MBP), PCs (κ and λlight chain), B cells (B220) and stromal cells (RFP) are displayed. Please click here to view a larger version of this figure.

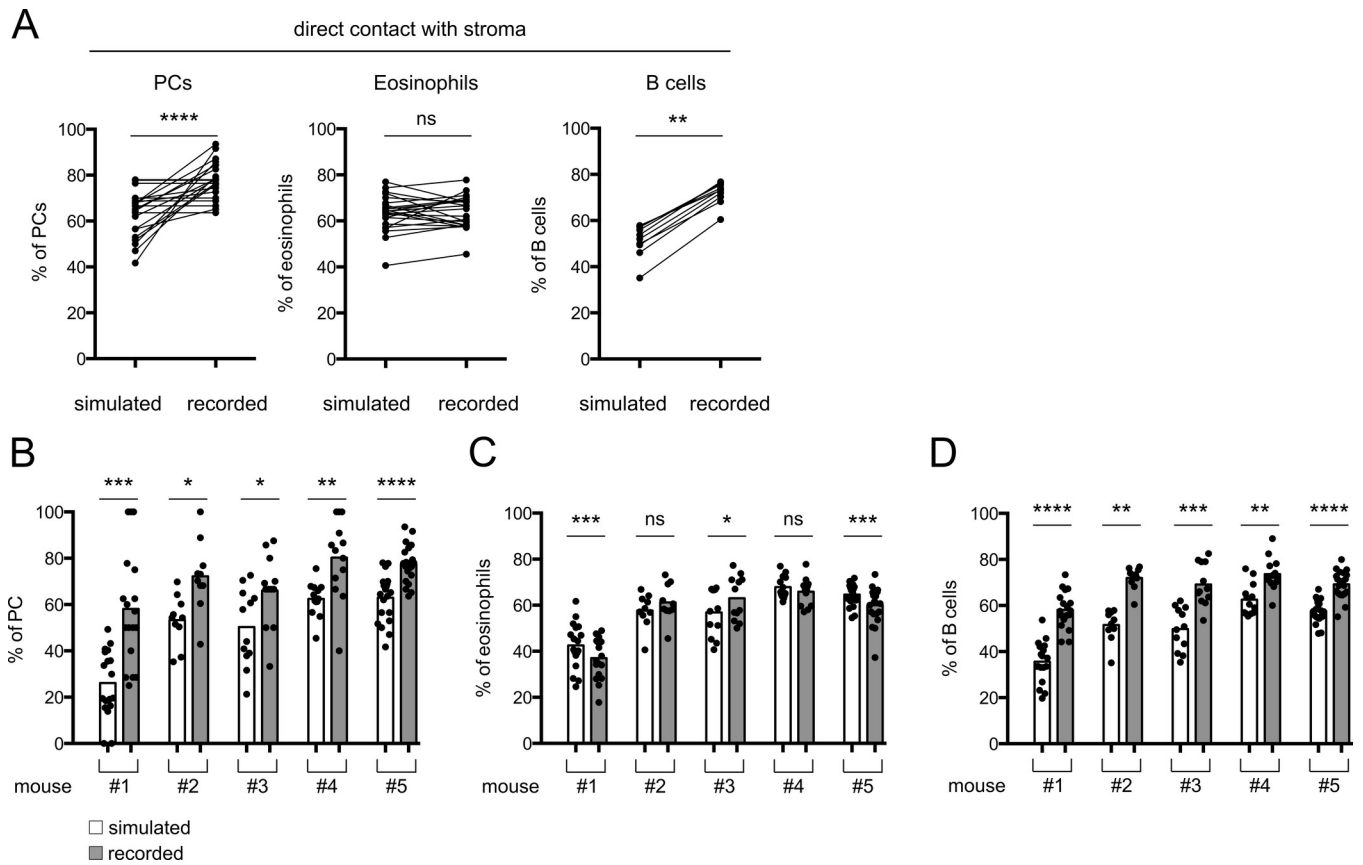

Figure 7. Direct contact of hematopoietic cell types with stromal structures in recorded vs. simulated images. (A) Frequency of PCs, eosinophils and B cells in direct contact with stroma in simulated compared to recorded images of fluorescent chimeric mice on day 30 after the boost. Lines connect corresponding simulated and recorded images (dots). Images of one representative mouse are shown in each plot. **(B)** Frequencies of PCs, eosinophils and B cells in direct contact with stroma in simulated compared to recorded images of 5 individual mice from two independent experiments. Wilcoxon signed rank test, two-tailed (PCs: ***p = 0.0001; *p = 0.0371; *p = 0.0161; **p = 0.0012; ****p < 0.0001; eosinophils: ***p = 0.0007; p = 0.1055; *p = 0.0161; p = 0.4143; ***p = 0.0007; B cells: ****p < 0.0001; **p = 0.0020; ***p = 0.0005; **p = 0.0012; ****p < 0.0001). Dots represent individual images. Bars indicate mean. P values 0.05 are considered significant differences. Asterisks in figures indicate the following P values: ns: p > 0.05; *: p 0.05; **: p 0.01; ***: p 0.001; ****: p 0.0001. Parts of this figure (direct contact of PCs with stromal structures) are modified from Zehentmeier *et al.*[9] Please click here to view a larger version of this figure.

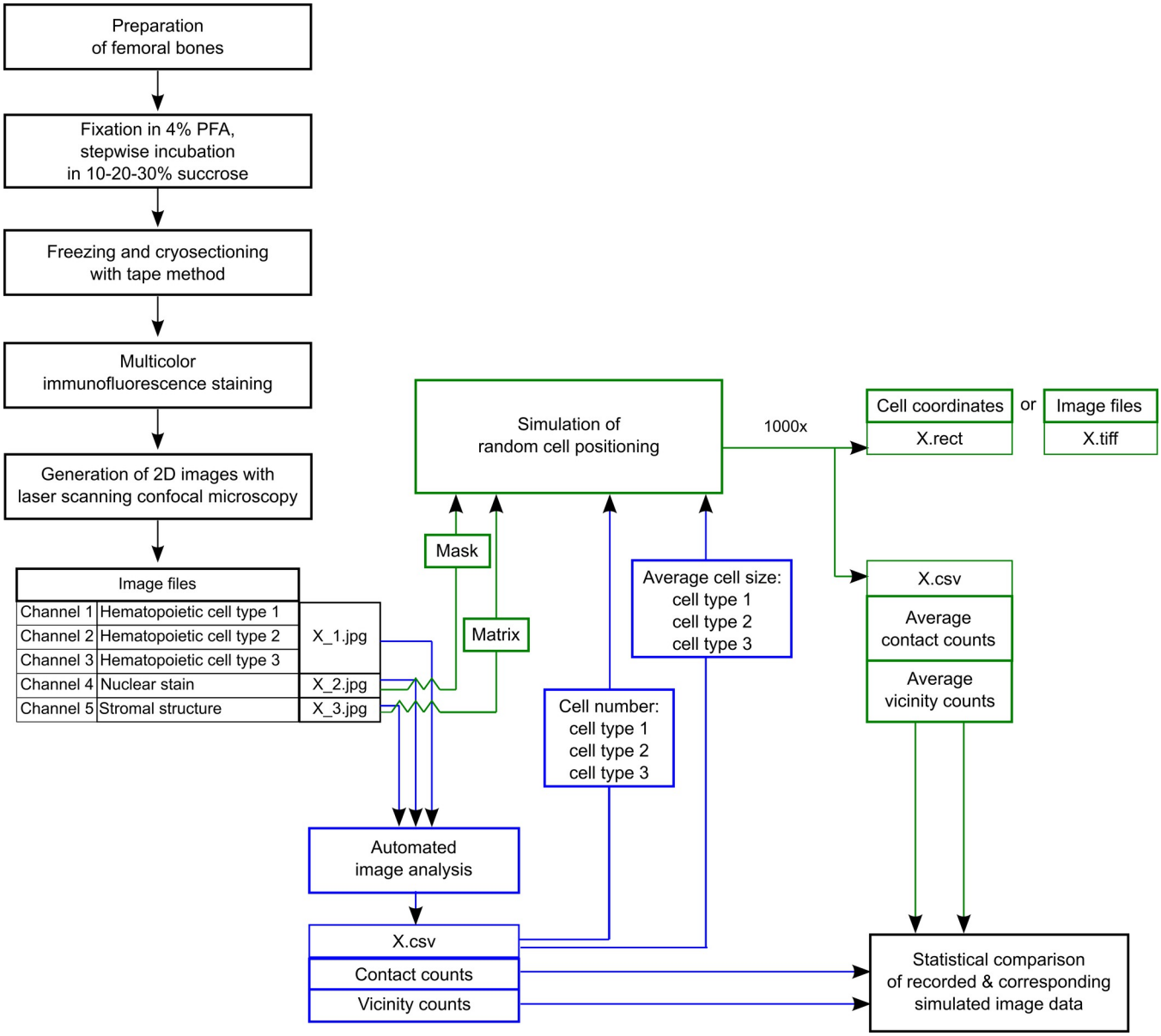

Figure 8. Complete workflow of the quantification approach for hematopoietic cell – stromal cell interactions in murine bone marrow. The approach is divided in three major parts: 1. murine bone marrow sections are prepared and raw data is collected by laser scanning confocal microscopy, 2. the automated analysis of the recorded images and the simulation of random positioning of bone marrow cells is performed, 3. the contact and neighborhood counts obtained from recorded and simulated images are compared. The input (image files) and output (text file) of the automated analysis is indicated in blue, the input (image files) and output (text files and, optionally, image files) of the simulation tool is indicated in green. Please click here to view a larger version of this figure.

Discussion

Despite the progress in modern optical imaging methods, the analysis of histological data is still often hindered by the lack of proper quantification tools and methods, or by biased analyses that focus on a small area of interest. The synergistic approach presented here combines image analysis covering the entire bone marrow region, automated segmentation and object recognition of various hematopoietic and stromal cell types, co-localization analysis, and finally a validation tool of non-randomly occurring contacts provided by a new custom-designed simulation software.

Histology of whole bones including the bone marrow has been difficult to perform due to the various tissue densities present in one section – on the one hand the very hard, mineralized bone, on the other hand the extremely fragile marrow, which gets easily disrupted when cut together with the bone. As an alternative, the tape method for cutting bone sections presented here[14,15] has the advantage that it stabilizes the tissue, thereby leaving the endosteal areas intact (**Figure 1**). Besides being rich in osteoblasts, these areas have been suggested to play a role in stem cell maintenance[20].

The crucial role of stromal cells in developmental processes and cellular maintenance in the bone marrow is becoming increasingly evident. However, the analysis of these rare, fragile cells has proven to be difficult for two reasons: first, they are difficult to isolate from the bone marrow; second, the degree of heterogeneity among the stromal population is not known, and therefore one might miss an important population by using certain markers that have been described for stromal cells. The method to generate fluorescent bone marrow chimeras is useful to fluorescently mark and subsequently analyze the bone marrow stromal cell population as a whole. However, it should be noted that in these mice all mesenchymal cells of the bone marrow are visualized, including endothelial cells and osteoblasts. This needs to be taken into account if data from such chimeric mice is analyzed. Even though there is also a risk of hematopoietic cells of recipient origin surviving the irradiation, these cells typically only cover a very small area per field of view compared to the donor $CD45^+$ cells, thus not affecting the histological analysis[9]. Clearly, this method should be combined in a subsequent step with a more specific detection of stromal (sub)populations. Currently, the analysis of these cells is mostly done by histology due to the reasons mentioned above, imposing a limit on the number of parameters that can be analyzed at the same time. The development of multi-parameter analyses in microscopy will help to overcome these limits.

During image analysis, the segmentation was performed using the original Otsu's algorithm. Essentially, this clustering-based thresholding method automatically determines the intensity threshold for the optimal separation of the foreground (signal) and background (noise) pixels into two groups with the lowest statistical divergence in a given channel, resulting in a binary image[17]. Here, Otsu's method was applied to the natural logarithm version of the original image, that is:

Input image for Otsu = ln(Input image)

This works better for fluorescence images since Otsu's method may identify dim cells as background. Adding the logarithmic function allows for a better separation of the cells and background into two different classes by Otsu's algorithm. However, intensity thresholding alone is not enough to precisely detect single objects. It works efficiently when detecting well-separated objects in images, but it is not sufficient to separate single cells located within clusters. As some of the cell types that were of interest for us, such as eosinophils or B cells, are frequently clustered together in the tissue, their nuclei in the DAPI channel were segmented using an algorithm based on the k-means clustering of the intensity histogram with k = 10 [21]. The cell segmentation algorithm will plot the brightest to the dimmest pixels (clustered in 10 bins) and constantly look for the formation of cell-resembling objects. These objects will then be defined as cells. When all pixels have been used, the resulting nuclei are dilated to generate a mask that is then applied to the other channels for cluster separation.

It should be noted that this analysis works well for hematopoietic cells that are compact, but that it is limited with respect to stromal cells, as it is not possible to determine the borders of these large, spread-out cells due to the interconnection of their dendritic extensions that form a reticular network. Thus, cell counts for stromal cells cannot be provided. Labeling single cells via fate-mapping reporters under the control of stroma-specific promoters will solve this issue, according to what has been published for neurons (using the "Brainbow" system[22]) and for the labeling of follicular dendritic cells in the lymph nodes[23].

In addition to applying a noise reduction step to all channels by excluding objects below 30 px, size exclusion was applied in the process of object recognition for hematopoietic but not stromal cells. Small fragments of cells that were cut by sectioning may be excluded; however, the loss can be neglected in this case in favor of an unambiguous recognition of the cells. Extending the analysis and simulation from two to three dimensions will overcome this limitation. The development of methods to study cellular distribution in whole mounts, *e.g.,* by multi photon microscopy or light sheet microscopy/SPIM, will certainly help in this respect. In order to study the complex cellular composition of multi-component niches, it will also become necessary to extend the number of parameters that are being analyzed *in situ*. Promising approaches for multiparameter analysis of histological information in combination with cytometric quantification have been published recently[24,25].

The contact analysis was performed by quantifying the overlap of two objects. Direct contact was defined as an overlap of at least one pixel. Importantly, this analysis is limited by the resolution of the microscopy images and therefore depends on the wavelength and mode of excitation, as well as on the numerical aperture of the objective lens used in the microscope, and the pinhole size. In the analysis shown here, a 0.8 NA, 20X objective with fluorochrome combinations excited with 488, 561, 594, and 633 nm using one photon excitation was applied. Hence, lateral resolution values between 0.372 and 0.483 µm were achieved. This allows assertions to be made about the juxtaposition of various cell subsets; however, it does not give any information about putative molecular mechanisms involved in cellular interactions. Additionally, other methods such as 2-photon intravital microscopy are needed to improve the characterization of these intercellular contacts[9]. Förster-resonant energy transfer (FRET)-based systems can help to confirm if these interactions are actually functional[26].

In order to evaluate the cellular microenvironment of tissue niches, it is not only crucial to analyze the direct cell contacts, but also to quantify the cell types in the neighborhood of a certain cell type of interest ("vicinity analysis"). Previously published studies measured distances between cells and tissue structures such as vessels based on the position of the nucleus[27]. Since we were interested in determining the distance of various cell types, in part with varying ratios of nuclear to cytoplasmic volume, we preferred to measure the distance between surfaces. To this end, we calculated the vicinity radius by determining the Euclidian distance from a cell´s boundary after converting the values from µm to px. The Euclidean distance is the straight-line distance between two pixels and can be described by the formula[28]:

$$(for\ points\ a\ and\ b):\ distance\ = \sqrt[2]{(x_b - x_a)^2 + (y_b - y_a)^2}$$

Cells with pixels of their boundaries within an Euclidean distance of *e.g.,* 10 µm from the pixels of a target cell's boundaries were counted as neighboring this cell.

In its current form, the analysis only determines whether a cell is contacted or approached by another cell of the same or different type, thus providing only a binary YES/NO characterization. The actual number of cells that contact the cell of interest or are within a certain radius from it is not calculated. The next step will be to extend the current analysis in a way that the group size of contacting or neighboring cells can be detected and compared between different target cells of the same type. This will lead to important additional information about the composition of bone marrow niches, such as the survival niche for bone marrow plasma cells, for which a varying contribution of hematopoietic accessory cells has been discussed[29-33].

The object recognition algorithms were optimized together with the specialists from Wimasis using their commercially available custom solution service and are available upon request. Another option is to use either commercially available software for image analysis, such as Definiens, Volocity, or Imaris, or freeware such as CellProfiler.

The automated cell segmentation and image analysis tools were validated by comparing their results with manually analyzed data provided by 6 trained image raters with respect to two parameters, namely the object size and the number of cells in various cell populations. As shown in **Figure 3B**, the average object size for hematopoietic cells (PCs, eosinophils, and B cells) was similar between both methods, with a higher variance for manual size determination for plasma cells and eosinophils, probably due to their more irregular shape compared to B cells. The automated detection of cell numbers yielded slightly lower values than the manually detected ones. Notably, they were still within the range of the manual values in the case of eosinophils and PCs, while they were below these values in the case of B cells, probably due to a higher heterogeneity of expression of B220, which was used as a marker for B cells. B220 is known to be up-regulated during B cell differentiation in the bone marrow, and B cells with low as well as high intensity staining for B220 can be observed. B cells with low B220 signals fell below the applied threshold, which may have led to the exclusion of the earliest-stage B cells. A lower threshold for the automated detection may solve this issue. For stromal cells, which are harder to detect due to their less compact, more dendritic, and stretched-out morphology, the manual detection resulted in high variances between individual raters. Interestingly, the average total area of stroma was equal to the total area determined automatically, indicating that the analysis is well suited to compensate for individual bias by the raters. Taken together, these data show that the automated results generally represent the average values of manual analyses and are well suited to reduce interrater variability in the analysis.

In order to discriminate random and non-random positioning of cells within the structural limitations of the tissue, a simulation tool was developed. During the simulation, an artificial image with randomly positioned hematopoietic cells is created for every recorded bone marrow histological image. First, the stroma channel image is utilized in its original format. A mask is generated from the DAPI image by applying a fixed intensity-based threshold, thus converting the image into binary format; the binary mask then undergoes multiple steps of pixel-based dilation and erosion. The mask defines areas in the image field where simulated cells are allowed to be placed. The coordinates of the centers of the simulated cells are provided by an uniform random number generator, the boundaries of which where determined by the image size. Information about the cell number and average cell size for each population determined by automated image analysis of the recorded images are used to define the simulated hematopoietic cell populations. The simulated cell diameter is assumed to follow a one-dimensional Gaussian distribution from which the actual cell diameter is selected randomly: The diameter is then modified so that cell size cut-offs for the minimum allowable object size are introduced. In case the simulated cell would be positioned such that one or more pixels overlap with a no-go area or would be within a predefined distance from another already placed cell (4 µm from center to center as determined in recorded images), new random coordinates will be chosen whilst the diameter is left unaltered. This will be repeated until the number of simulated cells equals the number of cells in the recorded image.

The tool was based on the assumption that hematopoietic cells can be positioned freely within the bone marrow, while stromal structures act as a fixed matrix within the tissue. The tool was optimized to the situation in the bone marrow where parenchymal areas are crossed by a complex system of sinusoids. A similar modeling approach was recently published by Frenette and co-workers in order to analyze the positioning of hematopoietic stem cells in relation to stromal cells and vascular structures, which make up about 30% of the total femoral bone marrow volume[25]. In order to correct for this effect, the simulation tool presented here is based on a mask of areas were cells are allowed to be placed. This was achieved by using a nuclear stain image, in which the objects representing the nuclei were expanded by a 5-step dilation (see **Figure 6**) after binarization. Areas with a low cellular density, *i.e.,* low density of nuclei such as bone and sinusoids, will not contribute to the mask and therefore become no-go areas. In order to avoid an artificial reduction of these no-go areas by the dilation procedure, a 5-step erosion was applied subsequently, thus reopening larger exclusion areas, whilst leaving the high nuclear density (hence “allowed”) areas unaltered. This method can be easily adapted for other lymphoid organs. In those tissues were this method might not work (*e.g.,* in areas where cells with a high cytoplasm/nucleus ratio are present), other methods such as cytoplasmic labeling can be used to create the mask.

Hematopoietic cells were simulated as circular objects whose size was determined by using a Gaussian random number generator, the mean of which agreed with the calculated average diameter of each cell type. The width of the distribution was based on measured cell size distributions in recorded images as determined by an image analysis software. In order to take into account that small cellular fragments were excluded in the automated image analysis, cell size cut-offs were introduced as determined from the measured cell size distributions for each cell type (see **Figure 5**).

Naturally, this works well for cell types that are relatively uniform in their size and shape but may lead to problems in the case of cells that are highly heterogeneous with respect to these parameters. It should be noted that this analysis is optimized for the major hematopoietic cell types in the bone marrow (granulocytes, hematopoietic progenitors and lymphocytes), which have in common that they possess a regular, nearly rounded shape. However, this method has not been tested for dendritic cells or macrophages, cell types with strongly irregular cell bodies. Analyzing such cells will present new challenges to our automated image analysis as well as to the simulation approach, including the need for improved cell cluster separation algorithms[24] as well as detailed shape-analysis and simulation of not only differently sized but also differently shaped cells. An alternative would be a simulation approach that works with the exact shapes as recorded. However, it must be noted that this method would significantly increase the deterministic behavior of the model system.

For the simulated experiments, 1,000 repetitions of the simulation for every recorded image were generated. Using this many repetitions will reduce the relative error contributed by the simulation process itself to about 3%. Namely, if the cell-cell co-localization values are calculated from simulations that are random, then the simulation process itself will be characterized by an $N^{-1/2}$ error function, where N is the number of simulations per measured image. This is the contribution by the simulation process itself to the accumulated error of the measured co-localization values. Thus, for N = 1,000 the contributed error is 3.16%. The simulations shown here ran for 20 to 60 min per image per 1,000 repetitions when only saving the simulated images as .rect files (a simple text format) rather than as actual images in .jpeg or .tiff format (also an option in the software).

Taken together, this approach allows for an unbiased, high-throughput analysis of histological images and enables the generation of statistically relevant data. This may be useful in comparing cellular localization under different conditions. Moreover, the temporal component can in the future be integrated into a modeling approach of bone marrow cell movements, as more data on the motility of various cell types in the bone

marrow becomes available. This method can then be used to simulate perturbations of the system, such as the mobilization of cells from the bone marrow into the circulation, *e.g.,* neutrophils in the case of an acute inflammation[34]. To further elucidate the function of the bone marrow as a storage place for immune memory cells, one can also imagine extending it to model the competition for survival factors. Also, the possible crosstalk between distinct niches could be addressed, as well as the induction of niches. Together, this will help to understand the physiological changes (*e.g.,* triggers for regenerative behavior in stem cells) as well as the pathological perturbations of the system as a whole, for example in the case of autoimmune disorders, neoplasia, or acute inflammation. As part of an iterative concept of experiment and modeling, new hypotheses can be generated based on the simulations, which in turn can again be tested experimentally, thereby helping to further understand the function and interaction of various cell types within the complexity of tissues.

Disclosures

Juan Escribano Navarro is affiliated with Wimasis GmbH, Munich, Germany. The other authors have no conflicts of interest to declare.

Acknowledgements

We thank Andreas Radbruch for valuable discussions. We are grateful to Sabine Gruczek, Patrick Thiemann and Manuela Ohde for assistance with animal care and Robert Günther for excellent technical assistance. We thank our trained raters Laura Oehme, Jannike Bayat-Sarmadi, Karolin Pollok, Katrin Roth, Florence Pache and Katharina Horn for evaluation of the histology samples and Randy Lindquist for proofreading of the manuscript. We thank J. and N. Lee, Mayo Clinic, Scottsdale, Arizona, USA for MBP-specific antibodies.

This work was supported by DFG HA5354/4-1, by JIMI-a DFG core facility network grant for intravital microscopy and by TRR130/TP17,and DFG FOR 2165 (HA5354/6-1) to A.E.H. S.Z. was supported by the International Max Planck School for Infectious Diseases and Immunology (IMPRS-IDI), Berlin.

References

1. Kunisaki, Y., Frenette, P. S. The secrets of the bone marrow niche: Enigmatic niche brings challenge for HSC expansion. *Nat Med.* **18**, 864-865 (2012).
2. Morrison, S. J., Scadden, D. T. The bone marrow niche for haematopoietic stem cells. *Nature.* **505**, 327-334 (2014).
3. Tokoyoda, K., Egawa, T., Sugiyama, T., Choi, B. I., Nagasawa, T. Cellular niches controlling B lymphocyte behavior within bone marrow during development. *Immunity.* **20**, 707-718 (2004).
4. Cariappa, A., *et al.* Perisinusoidal B cells in the bone marrow participate in T-independent responses to blood-borne microbes. *Immunity.* **23**, 397-407 (2005).
5. Sapoznikov, A., *et al.* Perivascular clusters of dendritic cells provide critical survival signals to B cells in bone marrow niches. *Nat Immunol.* **9**, 388-395 (2008).
6. Tokoyoda, K., *et al.* Professional memory CD4+ T lymphocytes preferentially reside and rest in the bone marrow. *Immunity.* **30**, 721-730 (2009).
7. Mazo, I. B., *et al.* Bone marrow is a major reservoir and site of recruitment for central memory CD8+ T cells. *Immunity.* **22**, 259-270 (2005).
8. Lin, G. H., *et al.* Contribution of 4-1BBL on radioresistant cells in providing survival signals through 4-1BB expressed on CD8(+) memory T cells in the bone marrow. *Eur J Immunol.* **42**, 2861-2874 (2012).
9. Zehentmeier, S., *et al.* Static and dynamic components synergize to form a stable survival niche for bone marrow plasma cells. *Eur J Immunol.* **44**, 2306-2317 (2014).
10. Nagasawa, T. Microenvironmental niches in the bone marrow required for B-cell development. *Nat Rev Immunol.* **6**, 107-116 (2006).
11. Luche, H., Weber, O., Nageswara Rao, T., Blum, C., Fehling, H. J. Faithful activation of an extra-bright red fluorescent protein in 'knock-in' Cre-reporter mice ideally suited for lineage tracing studies. *Eur J Immunol.* **37**, 43-53 (2007).
12. Schwenk, F., Baron, U., Rajewsky, K. A cre-transgenic mouse strain for the ubiquitous deletion of loxP-flanked gene segments including deletion in germ cells. *Nucleic Acids Res.* **23**, 5080-5081 (1995).
13. Kawamoto, T. Use of a new adhesive film for the preparation of multi-purpose fresh-frozen sections from hard tissues, whole-animals, insects and plants. *Arch Histol Cytol.* **66**, 123-143 (2003).
14. Kawamoto, T., Kawamoto, K. Preparation of thin frozen sections from nonfixed and undecalcified hard tissues using Kawamot's film method. *Arch Histol Cytol.* **1130**, (2012), 149-164 (2012).
15. Smith, C. L., *et al.* Basic confocal microscopy. *Current protocols in neuroscience / editorial board, Jacqueline N. Crawley ... [et al.].* **2**, (Unit 2.2), (2001).
16. Otsu, N. A threshold selection method from gray-level histograms. *IEEE Trans. Sys., Man., Cyber.* **9**, 62-66 (1979).
17. Hughes, I., Hase, T. *Measurements and Their Uncertainties: A Practical Guide To Modern Error Analysis.* Oxford University Press Oxford, UK (2010).
18. Quinn, G. P., Keough, M. J. *Experimental Design and Data Analysis for Biologists.* Cambridge University Press Cambridge, UK (2002).
19. Kiel, M. J., Morrison, S. J. Uncertainty in the niches that maintain haematopoietic stem cells. *Nat Rev Immunol.* **8**, 290-301 (2008).
20. MacQueen, J. B. Some Methods for classification and Analysis of Multivariate Observations. *Proceedings of 5th Berkeley Symposium on Mathematical Statistics and Probability Vol. 1.* 1965 Jun 21-Jul 18, Statistical Laboratory of the University of California, Berkeley, 666 University of California Press Berkeley, CA (1967).
21. Livet, J., *et al.* Transgenic strategies for combinatorial expression of fluorescent proteins in the nervous system. *Nature.* **450**, 56-62 (2007).
22. Jarjour, M., *et al.* Fate mapping reveals origin and dynamics of lymph node follicular dendritic cells. *J Exp Med.* **211**, 1109-1122 (2014).
23. Gerner, M. Y., Kastenmuller, W., Ifrim, I., Kabat, J., Germain, R. N. Histo-cytometry: a method for highly multiplex quantitative tissue imaging analysis applied to dendritic cell subset microanatomy in lymph nodes. *Immunity.* **37**, 364-376 (2012).
24. Moreau, H. D., *et al.* Dynamic in situ cytometry uncovers T cell receptor signaling during immunological synapses and kinapses in vivo. *Immunity.* **37**, 351-363 (2012).

25. Siffrin, V., *et al.* In vivo imaging of partially reversible th17 cell-induced neuronal dysfunction in the course of encephalomyelitis. *Immunity.* **33**, 424-436 (2010).
26. Shen, Q., *et al.* Adult SVZ stem cells lie in a vascular niche: a quantitative analysis of niche cell-cell interactions. *Cell Stem Cell.* **3**, 289-300 (2008).
27. Danielsson, P. E. Euclidian distance mapping. *Computer Graphics and Image Processing.* **14**, 21 (1980).
28. Tellier, J., Kallies, A. Finding a home for plasma cells - a niche to survive. *Eur J Immunol.* (2014).
29. Winter, O., *et al.* Megakaryocytes constitute a functional component of a plasma cell niche in the bone marrow. *Blood.* **116**, 1867-1875 (2010).
30. Rozanski, C. H., *et al.* Sustained antibody responses depend on CD28 function in bone marrow-resident plasma cells. *J Exp Med.* **208**, 1435-1446 (2011).
31. Rodriguez Gomez, M., *et al.* Basophils support the survival of plasma cells in mice. *J Immunol.* **185**, 7180-7185 (2010).
32. Belnoue, E., *et al.* Homing and adhesion patterns determine the cellular composition of the bone marrow plasma cell niche. *J Immunol.* **188**, 1283-1291 (2012).
33. Kohler, A., *et al.* G-CSF-mediated thrombopoietin release triggers neutrophil motility and mobilization from bone marrow via induction of Cxcr2 ligands. *Blood.* **117**, 4349-4357 (2011).

